ORNL/TM-2023/3102

Progress on Design and Production of Oxide Dispersion–Strengthened Alumina-Forming Austenitic Alloys for Nuclear Applications

Caleb Massey
David Hoelzer
Yukinori Yamamoto
Tim Graening
Sebastien Dryepondt
Holden Hyer
Josh Kendall
Mike Zach

September 2023

M4FT-23OR060101044

OAK RIDGE National Laboratory

ORNL IS MANAGED BY UT-BATTELLE LLC FOR THE US DEPARTMENT OF ENERGY

ORNL/TM-2023/3102

Innovative Nuclear Materials Program

PROGRESS ON DESIGN AND PRODUCTION OF OXIDE DISPERSION–STRENGTHENED ALUMINA-FORMING AUSTENITIC ALLOYS FOR NUCLEAR APPLICATIONS

Caleb Massey
David Hoelzer
Yukinori Yamamoto
Tim Graening
Sebastien Dryepondt
Holden Hyer
Josh Kendall
Mike Zach

September 2023

M4FT-23OR060101044

Prepared by
OAK RIDGE NATIONAL LABORATORY
Oak Ridge, TN 37831
managed by
UT-BATTELLE LLC
for the
US DEPARTMENT OF ENERGY
under contract DE-AC05-00OR22725

CONTENTS

LIST OF FIGURES

LIST OF TABLES

ACKNOWLEDGMENTS

This research was sponsored by the US Department of Energy Office of Nuclear Energy's Innovative Nuclear Materials Program under contract DE-AC05-00OR22725 with UT-Battelle LLC. One of the alloys analyzed in this work was originally developed under the Powertrain Materials Core Program, Vehicle Technologies Office, Office of Energy Efficiency and Renewable Energy. The authors thank Mr. Ben Garrison for his thoughtful review of this report before publication and Daniel Newberry for his assistance with metallography.

ABSTRACT

Alumina-forming austenitic (AFA) alloys are a promising class of nuclear materials due to their high-temperature oxidation/corrosion resistance and mechanical properties. Unfortunately, these alloys are limited in use for core material applications, specifically in their use as nuclear fuel cladding. Improving these alloys through a fine dispersion of oxide precipitates and thus increasing the effective irradiation sink strength of the alloy system may mitigate many of the degradation phenomena expected during alloy deployment (such as high-temperature helium embrittlement for lead-cooled fast reactor applications). This work package has started using a combination of conventional and advanced manufacturing approaches to the fabrication of oxide dispersion–strengthened (ODS) AFA materials. As such, this report summarizes progress to date in the fabrication of new compositions of these ODS AFA materials with a focus on reactor-specific design and a multifaceted manufacturing approach. Two different compositions of AFA gas-atomized powders were procured, and 200 g of each have been prepared using mechanical alloying with the expectation of high-temperature consolidation in Q1 of FY24. In addition, an approach to use reactive cover gases to promote additional precipitate formation has been developed for implementation in FY24 as a direct comparison with conventionally manufactured alloys.

1. INTRODUCTION

Nuclear energy is at a crossroads, and many new nuclear reactor concepts look toward rapid qualification to address the rapidly growing demand for carbon-neutral energy solutions. Unfortunately, many of these concepts, including advanced lead-cooled fast reactors (LFRs) and heat pipe microreactors, will require materials with high creep strength, irradiation resistance, and resistance to oxidation and corrosion in the presence of coolants including air, supercritical CO_2, and lead. Fortunately, alumina-forming austenitic (AFA) stainless steels are a class of fully face-centered cubic (fcc) iron-based alloys designed for use in extreme environments requiring oxidation resistance at high temperatures. Originally designed in the early 2000s for use in fossil power generating systems (boiler tubing, steam turbine components, etc.), this class of alloys was designed with increased levels of aluminum addition to form a passive aluminum oxide scale instead of the conventional chromium oxide scales normally formed on conventional stainless steels [1].

Significant repositories of data on fossil-grade AFAs have been produced over the past decade (particularly with reference to oxidation and creep strength), and recently a subset of these alloys is being considered as a structural material candidate for advanced reactor applications including in the LFR [2]. Unfortunately, it is yet to be seen whether AFAs, which do have a high density of intermetallic and carbide precipitates depending on composition, have sufficient sink strength to balance increased helium generation (and thus postulated increases in cavity swelling) due to the higher nickel content of this alloy system.

In parallel to recent developments relevant to advanced reactors, increased concerns regarding irradiation hardening and embrittlement of body-centered cubic (bcc) FeCrAl alloys [3] have resulted in the scoping of a special subclass of light-water reactor (LWR)–relevant AFAs as a potential accident-tolerant fuel cladding. Unfortunately, however, irradiation-induced loss of ductility and decreases in fracture toughness are not solely a bcc-material issue, so it is still unclear whether conventionally designed AFAs will show beneficial performance in conventional LWR environments.

Irrespective of the final application, AFAs in their current wrought form have promise as nuclear structural materials, but practical challenges remain for their implementation as core materials (fuel cladding). One potential approach to increasing AFA relevance to core material applications is to increase the number density of nanoscale features that serve as recombination sites for irradiation-induced defects (aka *sinks*). If the sink strength of this material class can be readily increased, it may help mitigate concerns such as high-temperature helium embrittlement (HTHE) and enable AFAs to be used as a core material in LFRs. An increased sink strength will also increase creep strength and further increase the viability of this material system as a potential accident-tolerant LWR fuel cladding by increasing safety margins (burst temperature) in the event of a loss-of-coolant accident (LOCA) scenario. If these gains can be realized, then the use of ODS AFA would rapidly expand the design space of various nuclear reactor concepts as illustrated in Figure 1.

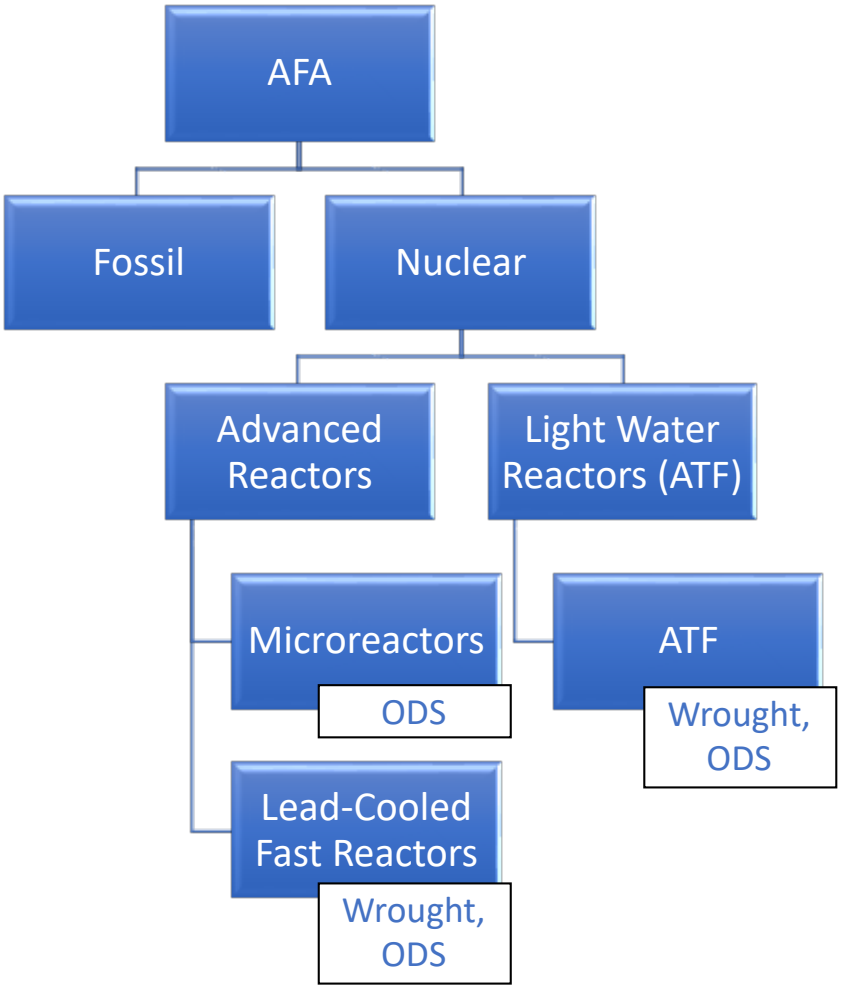

Figure 1. Applicability chart for AFA alloys. Prior applications can be expanded to be core and structural materials for both LWRs and advanced reactors.

The design of high sink strength oxide dispersion–strengthened (ODS) AFA variants is thus pursued in this work package for eventual tube production for fuel cladding production. The design strategy consists of (a) thermodynamic and neutronic design of AFAs with reactor-specific compositions, (b) demonstration of laboratory-scale ODS AFA production using conventional ODS alloy fabrication technologies, and (c) expansion of the ODS AFA processing window by using advanced manufacturing, as shown in Figure 2. The use of conventional manufacturing as a prerequisite to modern manufacturing approaches is necessary to establish a gold-standard baseline for the sink strength achievable in the ODS AFA with a combination of intermetallic, carbide/nitride, and oxide precipitate dispersions. Then, using in situ reactive element oxidation during melting/solidification, it is desired for the time-consuming mechanical alloying step to be removed from ODS AFA alloy production altogether to create a near-net shape thick-walled tube for subsequent pilger processing into a thin-walled geometry.

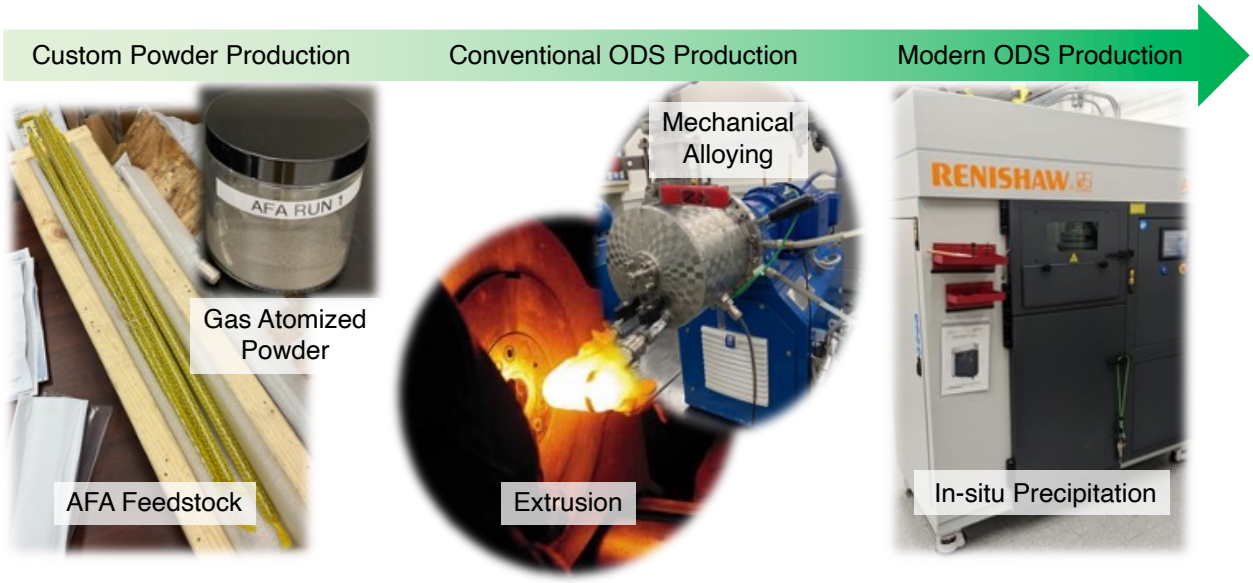

Figure 2. ODS AFA design strategy implemented in this work package. Following custom powder production, conventional ODS AFA strategies (mechanical alloying followed by high-temperature consolidation) will be produced to create a sink strength target for modern manufacturing to exceed.

In this report, recent progress in powder design, procurement, mechanical alloying, and consolidation is summarized. Then, a timeline for FY24 alloy production and characterization activities are presented.

2. REACTOR-SPECIFIC ALUMINA-FORMING AUSTENITIC COMPOSITIONS

Two AFA powder compositions were chosen for initial scoping for this project. The specifications for each and the measured compositions using a combination of inductively coupled plasma mass spectroscopy, inert gas fusion, and combustion analysis are listed in Table 1. The first alloy, titled *AA11* in this work, was designed for LWR applications, and the second alloy, titled *VA05*, is initially selected for LFR applications.

Table 1. Specified chemical compositions of gas-atomized AFA powder used in this work. The compositions are in weight percent as provided in supplier material certifications.

Element	LWR (AA11)		LFR (VA05)	
	Specification (wt %)	Measured (wt %)	Specification (wt %)	Measured (wt %)
Fe	bal.	bal.	bal.	bal.
Ni	25.0	25.0	22.0	23.0
Cr	16.0	16.0	17.5	17.6
Al	5.0	5.0	4.0	4.0
Mn	0.2	0.2	2.0	2.0
Mo	2.0	1.9	1.0	0.98
W	0.0	0.0	0.5	0.5
Si	0.2	0.2	0.5	0.4
Nb	1.5	1.4	0.7	0.7
Zr	0.0	0.0	0.10	0.13
Y	0.03	0.03	0.10	0.10
C	0.030	0.020	0.500	0.500
B	<0.01	0.000	0.010	0.010

Although the specifics of each alloy are not delved into in this work, notable differences are worth mentioning between the two variants. First, due to the alloy design strategy utilizing the fully austenitic nature for high-temperature use, sufficient levels of fcc stabilizing elements are needed to produce the desired microstructure. For the AA11 alloy, the nickel content is increased to balance the (a) bcc stabilizing effects of chromium and aluminum and (b) decreases in fcc stabilizing manganese, which in LWR thermal neutron spectrums is a very strong neutron absorber. The other major difference between the two alloys is the use of only molybdenum as a solid solution strengthening element in the LWR variant, whereas both molybdenum and tungsten are used in the LFR variant. This is because in the thermal spectrum of LWRs, much of the added tungsten would transmute away over the alloy's lifetime. Finally, slight differences exist in reactive elements (Nb, Zr) and preexisting impurities (C) within each powder, which affect the types of strengthening secondary phases. The AA11 alloy, the major strengthening mechanism at high temperature, relies on Laves and B2 forming on the grain boundary to prevent the grain boundary sliding at high temperatures associated with the LOCA scenario. For the LFR alloy (VA05), the alloy was originally designed as a family of cast austenitic stainless steel that maximized the formation of secondary carbide $M_{23}C_6$ as a strengthening phase with consumption of M_7C_3 forming during the solidification process.

Because of these differences in composition, different equilibrium fractions of major phases (intermetallic, Laves, carbonitrides, etc.) exist for each at a given service temperature. Following initial processing trials, iteration of alloy compositions to optimize reactor-specific AFAs will continue. See Figure 3.

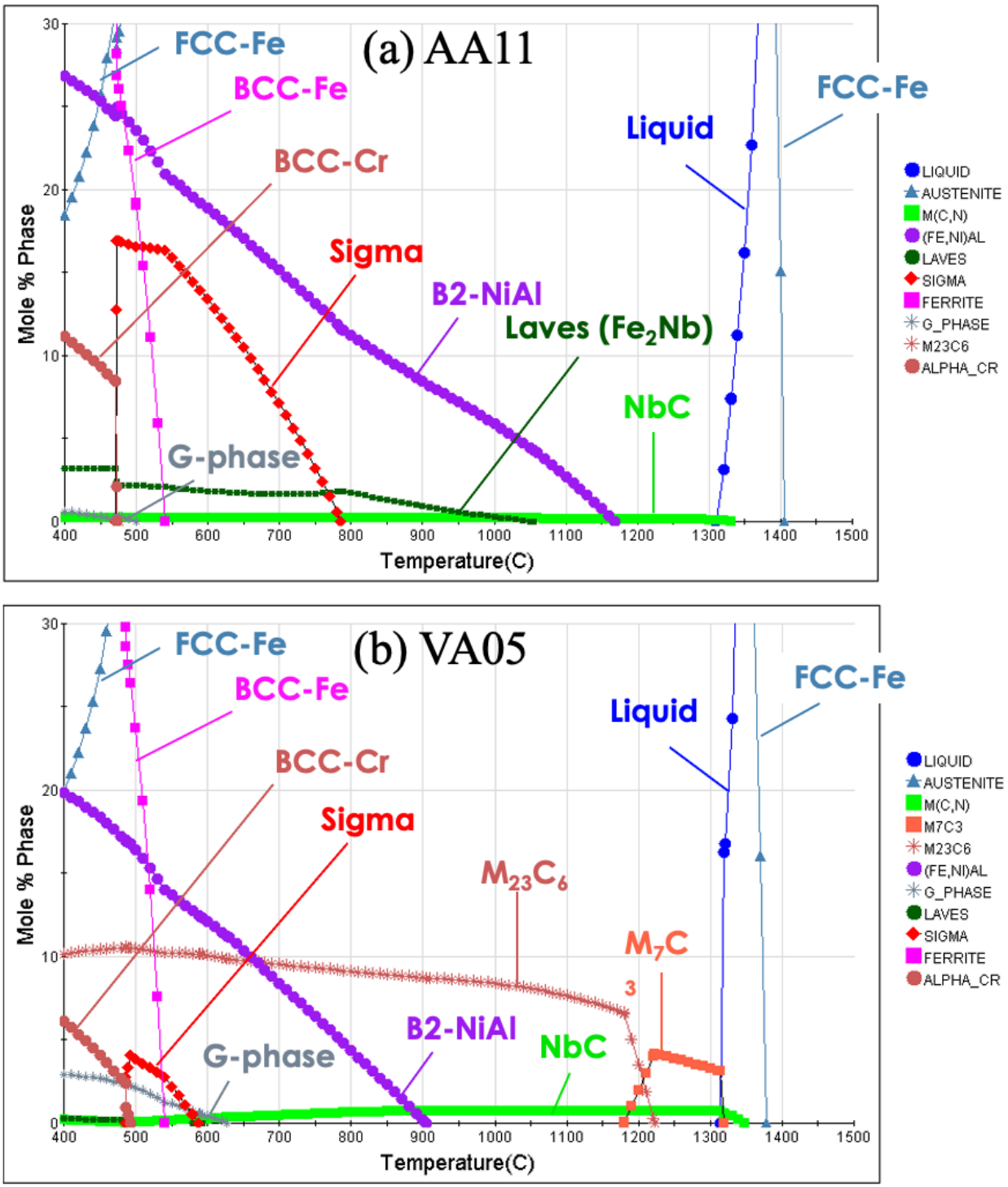

Figure 3. Phase diagrams for the LWR-focused (AA11) and LFR-focused (VA05) compositions used in this work (without subsequent additions of yttria).

3. OXIDE DISPERSION–STRENGTHENED ALUMINA-FORMING AUSTENITIC PRODUCTION VIA CONVENTIONAL MANUFACTURING

The two AFA powders were prepared using gas atomization. AA11 was produced initially in the form of 0.5 in. diameter bar feedstock produced by Sophisticated Alloys Inc. (Butler, Pennsylvania). The bar feedstock was then gas-atomized at Oak Ridge National Laboratory and sieved using a 300 μm mesh, resulting in approximately 600 g of AA11 powder for subsequent analysis and processing. Conversely, the second powder (VA05) was procured from Powder Alloy Corporation and received in gas-atomized form sieved to a +270 mesh (< 50 μm).

A Zoz Simoloyer attrition ball mill was used for initial powder mechanical alloying using mild-steel milling media and a ball-to-powder ratio of 10:1. Initial ball milling trials used the AA11 powder (mixed with 0.3 wt % Y_2O_3) milled with rotational speeds alternating from 400 to 900 rpm for 20 h in an argon atmosphere. Following mechanical alloying, however, the yield of the powder was only 10% (20 g of material per 200 g of initial powder loaded in the unit). This poor yield is common for the mechanical alloying of austenitic steels due to their high ductility and work hardening capacity, resulting in the slow accumulation of powder on the surface of the grinding media (Figure 4). This powder accumulation not only results in significant amounts of lost powder but also causes milling issues (the seizing of the ball mill) due to the increasing volume and surface roughness of the milling media as a function of time.

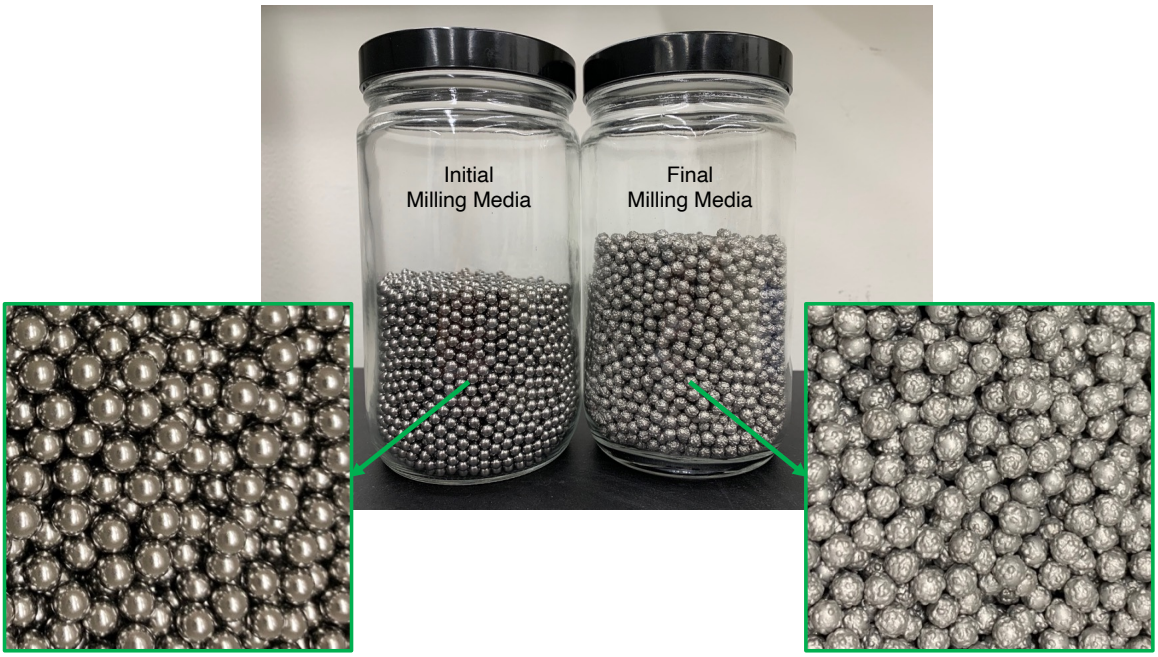

Figure 4. Evolution of milling media following ball milling, showing the growing surface coating of AFA particles on the surface of the mild-steel media.

The primary method normally used to increase the yield of highly ductile austenitic alloys during milling is the use of a process control agent (PCA). The most common ones are stearic acid and ethanol [4], but these usually cause a large contamination of carbon into the powder during mechanical alloying and require cumbersome extraction and drying procedures. Recent work has

also shown that milling in a nitrogen environment could serve a similar PCA purpose, and the resulting alloy had a fine dispersion of both oxygen- and nitrogen-rich precipitates [5, 6]. Unfortunately, this methodology may not be a prudent strategy for milling the current AFAs due to the much higher aluminum content of the alloys investigated here because it has been previously shown that nitrogen reacts with aluminum to form AlN, thereby removing valuable aluminum from the matrix that would otherwise form a protective alumina layer in the presence of oxidizing environments [7].

Avoiding PCAs, the powder yield is known to marginally increase as milling speed decreases [4]. So, the remaining 400 g of AA11 powder were milled for 20 h in an argon atmosphere at 300 rpm, resulting in a 60% yield (240 g of material). In addition, 400 g of VA05 powder were milled using the same conditions, resulting in a 66% yield (260 g of material). At these rotational speeds, the initially spherical powder particles begin to flatten into pancake morphologies by 5 h of milling (Figure 5 and Figure 6), followed by eventual cold welding into larger flat powder flakes by 20 h of milling. Future investigations that use scanning electron microscopy (SEM) with energy dispersive spectroscopy will evaluate the as-milled incorporation of the added Y_2O_3 powder in the powders. Following high-temperature consolidation, additional mechanical testing and lower length-scale characterization (transmission electron microscopy [TEM]) will reveal any inter- or intragranular precipitation.

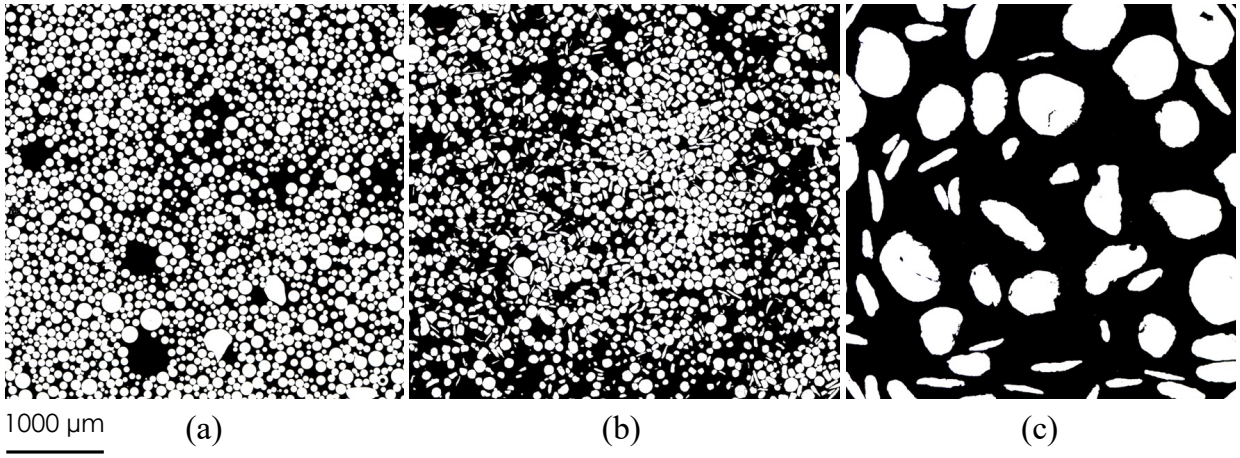

Figure 5. Evolution of AFA (AA11) powder after (a) 0 h, (b) 5 h, and (c) 20 h of mechanical alloying at 300 rpm in a Zoz Simoloyer ball mill.

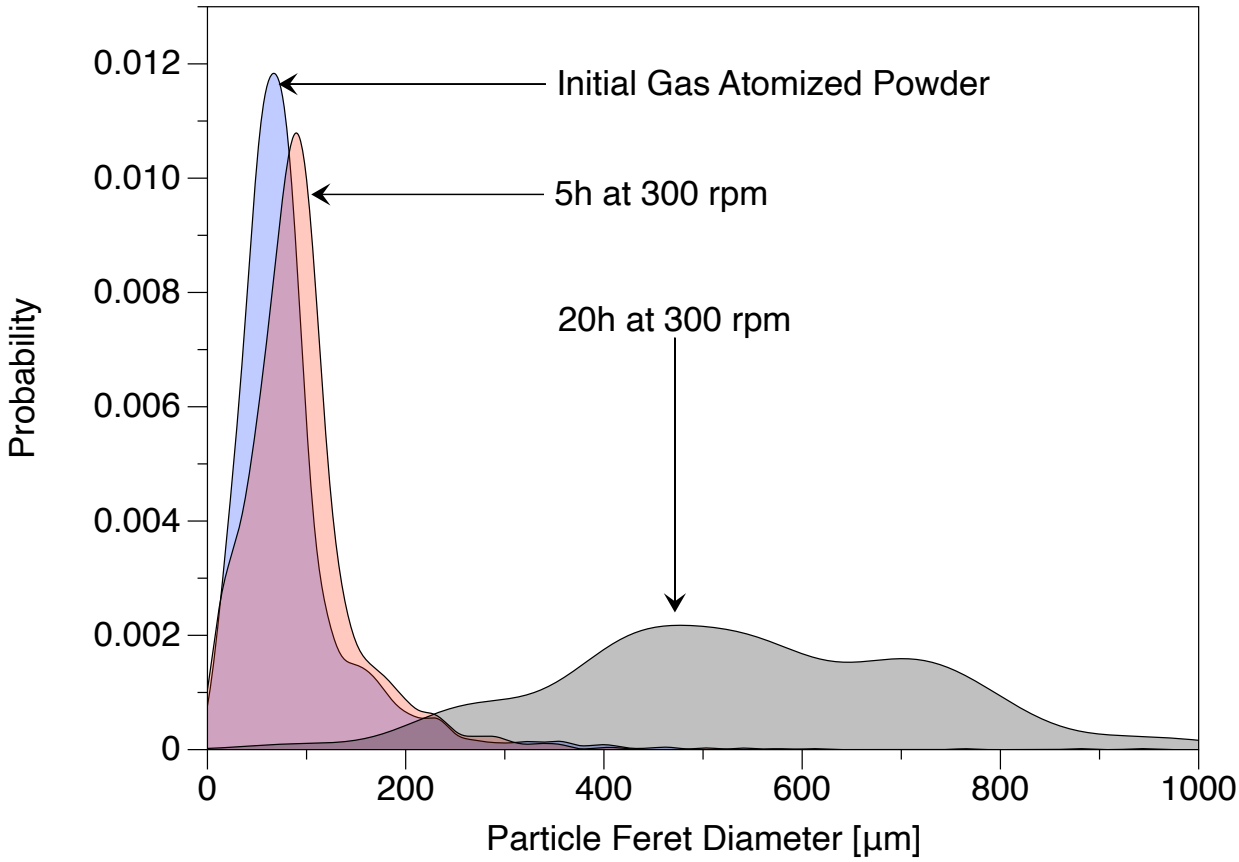

Figure 6. Evolution of AFA (AA11) powder after (a) 0 h, (b) 5 h, and (c) 20 h of mechanical alloying at 300 rpm in a Zoz Simoloyer ball mill.

4. A MODERN MANUFACTURING STRATEGY FOR OXIDE DISPERSION–STRENGTHENED ALUMINA-FORMING AUSTENITIC

Additive manufacturing of ODS steels has been researched within the past decade to overcome the issue of low number densities of oxide precipitates and/or the growth of precipitates during additive manufacturing [8]. Success of that research was limited, often failing to provide the required small precipitate sizes between 2 and 20 nm with high number densities of precipitates $>10^{22}$ m^{-3}. The correct sizes of precipitates have been shown using gas atomization reaction synthesis powder. That powder manages to keep the oxide precipitate forming rare earth elements nonoxidized during the gas atomization process. Then, during the additive manufacturing process, oxidation of intermetallic rare earth elements during additive manufacturing under an oxidizing environment (95% Ar + 5% O) has proven to result in the correct size of oxide precipitates [8]. However, the number densities during the additive manufacturing process were one to three orders of magnitude below the conventionally manufactured ODS steels [9-11]. The number of nanoscale precipitates is not only important to increase high-temperature creep performance but also critical for the ability to manage HTHE [5, 12, 13]. However, simply increasing the amount of precipitate-forming elements in the gas-atomized powder did not result in an increased number density; on the contrary, it led to an increase of precipitate size due to agglomeration of yttrium inside the gas-atomized powder.

Therefore, the idea to incorporate a second form of precipitates such as nitrides/carbides, as discussed in Section 3, must be considered. It was shown that nitrogen can be incorporated in steel powder during mechanical alloying to sequester nitrides during the extrusion process, resulting in dual precipitates [6]. Recently, additive manufacturing under a reactive atmosphere led to an increase of nitrogen inside the printed build [14]. These two key findings are crucial to increasing the number densities of nanoscale precipitates to achieve a binary size distribution of precipitates with oxides between 2 and 25 nm and nitrides with sizes between 20 and 60 nm. Oxides would mainly act as sinks for irradiation-induced defects (and He depending on neutron spectrum/fluence), while nitrides would enhance high-temperature creep properties. As mentioned previously, avoiding large amounts of aluminum nitride formation is critical to forming the alumina scale outside the build. Therefore, elements with a low Gibbs energy to form nitrides inside the material, such as zirconium and niobium, will be used to form carbides and/or nitrides during the laser powder bed fusion process by reacting with the nitrogen provided via the controlled printing atmosphere. A gas mixture of argon, nitrogen, and oxygen is suggested. Additionally, 5% of oxygen showed the most successful ODS precipitate production route, whereas the argon-to-nitrogen mixture would need to be gradually adjusted within the project to result in an optimized number density and size distribution of nitrides. Using other cover gases, such as CO_2, is also planned as an alternative to nitrogen-containing atmosphere to form a mixture of refined carbide and oxide precipitates throughout the AFA material. Some optimization is expected in FY24 to find a thermodynamically optimized combination of cover gas and AFA powder to produce nanoscale dual distributions of carbides/nitrides and oxides throughout the nanostructured AFA material.

The microstructure of printed parts will be investigated regarding grain size, precipitate size, and number density using SEM and TEM techniques. High-density builds with a promising microstructure will be compared with the conventionally produced ODS AFA.

5. CONCLUSIONS

This report summarizes recent efforts under the Innovative Nuclear Materials Program to produce ODS AFA for reactor fuel cladding applications. More specifically, FY23 work has produced mechanically alloyed ODS AFA powders of two different chemistries focused on both LWR and LFR applications. Weaknesses in the use of conventional approaches, such as the use of mechanical alloying, were revealed with only ~60% yield during mechanical alloying runs of gas-atomized AFA powders. In FY24, these powders will be consolidated into bars of ODS AFA material for microstructure and mechanical property evaluations. In addition, modern manufacturing techniques, specifically the use of laser powder bed fusion, will be employed using reactive cover gases to explore the processing space for ODS AFA material in reference to conventionally produced material.

6. REFERENCES

[1] Y. Yamamoto, M.P. Brady, Z.P. Lu, P.J. Maziasz, C.T. Liu, B.A. Pint, K.L. More, H. Meyer, E.A. Payzant, Creep-resistant, Al2O3-forming austenitic stainless steels, Science 316(5823) (2007) 433-436.
[2] B.A. Pint, Y.-F. Su, M.P. Brady, Y. Yamamoto, J. Jun, M.R. Ickes, Compatibility of Alumina-Forming Austenitic Steels in Static and Flowing Pb, Jom 73(12) (2021) 4016-4022.
[3] C.P. Massey, D. Zhang, S.A. Briggs, P.D. Edmondson, Y. Yamamoto, M.N. Gussev, K.G. Field, Deconvoluting the Effect of Chromium and Aluminum on the Radiation Response of Wrought FeCrAl Alloys After Low-Dose Neutron Irradiation, Journal of Nuclear Materials 549 (2021).
[4] M. Huang, J. Jiang, Y. Wang, Y. Liu, Y. Zhang, Effects of milling process parameters and PCAs on the synthesis of Al0.8Co0.5Cr1.5CuFeNi high entropy alloy powder by mechanical alloying, Materials & Design 217 (2022).
[5] T. Gräning, M. Rieth, J. Hoffmann, A. Möslang, Production, microstructure and mechanical properties of two different austenitic ODS steels, Journal of nuclear materials 487 (2017) 348-361.
[6] T. Gräning, M. Rieth, H. Leiste, M. Duerrschnabel, A. Möslang, On the mechanical alloying of novel austenitic dual-precipitation strengthened steels, Materials & Design 213 (2022).
[7] M.P. Brady, Y. Yamamoto, B.A. Pint, M.L. Santella, P.J. Maziasz, L.R. Walker, On the loss of protective scale formation in creep-resistant, alumina-forming austenitic stainless steels at 900 C in air, Materials Science Forum, Trans Tech Publ, 2008, pp. 725-732.
[8] T. Horn, C. Rock, D. Kaoumi, I. Anderson, E. White, T. Prost, J. Rieken, S. Saptarshi, R. Schoell, M. DeJong, Laser powder bed fusion additive manufacturing of oxide dispersion strengthened steel using gas atomized reaction synthesis powder, Materials & Design 216 (2022) 110574.
[9] L. Autones, P. Aubry, J. Ribis, H. Leguy, A. Legris, Y. de Carlan, Assessment of Ferritic ODS Steels Obtained by Laser Additive Manufacturing, Materials 16(6) (2023) 2397.
[10] S. Saptarshi, M. DeJong, C. Rock, I. Anderson, R. Napolitano, J. Forrester, S. Lapidus, D. Kaoumi, T. Horn, Laser Powder Bed Fusion of ODS 14YWT from Gas Atomization Reaction Synthesis Precursor Powders, JOM 74(9) (2022) 3303-3315.
[11] H. Jia, Z. Zhou, S. Li, A new strategy for additive manufacturing ODS steel using Y-containing gas atomized powder, Materials Characterization 187 (2022) 111876.

[12] J. Chen, P. Jung, T. Rebac, F. Duval, T. Sauvage, Y. De Carlan, M. Barthe, Helium effects on creep properties of Fe–14CrWTi ODS steel at 650° C, Journal of Nuclear Materials 453(1-3) (2014) 253-258.
[13] P. Edmondson, C. Parish, Q. Li, M. Miller, Thermal stability of nanoscale helium bubbles in a 14YWT nanostructured ferritic alloy, Journal of nuclear materials 445(1-3) (2014) 84-90.
[14] C. Cui, F. Stern, N. Ellendt, V. Uhlenwinkel, M. Steinbacher, J. Tenkamp, F. Walther, R. Fechte-Heinen, Gas Atomization of Duplex Stainless Steel Powder for Laser Powder Bed Fusion, Materials 16(1) (2023) 435.